3-D Zebrafish Embryo Image Filtering by Nonlinear Partial Differential Equations

Barbara Rizzi, Matteo Campana, Cecilia Zanella, Camilo Melani, Robert Čunderlik, Zuzana Krivá, Paul Bourgine, Karol Mikula, Nadine Peyriéras and Alessandro Sarti

***Abstract*— We discuss application of nonlinear PDE based methods to filtering of 3-D confocal images of embryogenesis. We focus on the mean curvature driven and the regularized Perona-Malik equations, where standard as well as newly suggested edge detectors are used. After presenting the related mathematical models, the practical results are given and discussed by visual inspection and quantitatively using the mean Hausdorff distance.**

I. INTRODUCTION

The biological processes leading to organism formation and development of individuals is a fundamental issue for the biomedical research but is nowadays largely not understood. Achieving of an integrated understanding of such processes needs to analyze the cells individually and in a living embryo. Such goal represents a challenge for imaging techniques and image processing algorithms. In fact, recent advances in imaging strategies open the way to *in toto* 3D+time imaging of live animals with a resolution at cellular level and enough contrast to allow segmentation and tracking of individual cells. However, a noise is intrinsically linked to the scanning technique and image analysis algorithms applied consequently to the time series of 3D zebrafish images need to remove spurious, noisy, structures. The image filtering has to be always a first step in a chain of image processing operations, and it is very important to design appropriate filters and chose their optimal parameters for any particular type of data. The goal of this paper is to apply the methods of nonlinear diffusion filtering to 3-D confocal images [1] of zebrafish embryogenesis in order to perform the segmentation [14] and the tracking [15] of individual cells. The filtering models are discussed in section II. Section III introduces a modified version of standard edge detector to filter membranes data. In section IV we analyse behavior of the methods in processing our 3-D data set. We evaluate quantitatively the filtering results using the mean Hausdorff distance of isosurfaces to a gold standard.

Manuscript received April 16, 2007.This work was supported by the European projects Embryomics and Bioemergence, promoted by the Sixt Framework Programme FP6-NEST (Embryomics: Project Reference 12916, NEST-2003-1 Adventure activities; BioEmergences: Project Reference 28892, NEST-2004-Path-IMP Measuring the Impossible).

B.Rizzi, M.Campana, C.Zanella, C.Melani and A.Sarti are with DEIS, Bologna University, Italy, brizzi@deis.unibo.it, mcampana@deis.unibo.it, cecilia.zanella2@unibo.it, camilo@dc.uba.ar, asarti@deis.unibo.it

R.Čunderlik, Z.Krivá and K.Mikula are with Department of Mathematics, Slovak University of Technology, Bratislava, Slovak Republic, cunderli@svf.stuba.sk;kriva@vox.svf.stuba.sk; mikula@vox.svf.stuba.sk

P.Bourgine is with CREA-Ecole Polytechnique, head of the Complex Systems Institute of Paris, and president of the European Complex Systems Society, paul.bourgine@polytechnique.org

N.Peyriéras is with DEPSN, CNRS, Institut de Neurobiologie Alfred Fessard, Gif-sur-Yvette, France. nadine.peyrieras@inaf.cnrs-gif.fr

II. NONLINEAR PDEs BASED MODELS

Let the input processed 3-D image be modelled by a real function $I_0(\mathbf{x})$, $I_0 : \Omega \to \mathbb{R}$, where $\Omega \subset \mathbb{R}^3$ represents a spatial rectangular domain. Observing that the Gauss function is a fundamental solution of the linear heat equation,

$$I_t = \Delta I = \nabla \cdot (\nabla I) \tag{1}$$

it has been possible [2], [3] to replace the classical convolution of an image with the Gaussian kernel of a given variance $v = \sqrt{2\sigma}$ by solving the linear heat equation for a corresponding time $t = \sigma$ and initial condition $I(\mathbf{x}, 0) = I_0(\mathbf{x})$. Applying (1) to an image means to diffuse its graylevels in an isotropic way. Despite the fact that (1) reduces the noise superimposed to the image, it blurs edges and moves their position. To overcome these shortcomings, Perona and Malik [4] introduced the first nonlinear diffusion model called *anisotropic diffusion* in the computer vision community

$$I_t = \nabla \cdot (g(|\nabla I|)\nabla I), \tag{2}$$

making the diffusion coefficient g dependent on the image features. This model can behave locally as the backward heat equation, depending on the intensity of $|\nabla I|$, which is an ill-posed problem from a matematical point of view. Therefore Catté, Lions, Morel and Coll [5], [6] proposed to use the convolution of ∇I with the Gaussian kernel to evaluate the diffusion coefficient, keeping all the advantages of the original model and avoiding its drawbacks

$$I_t = \nabla \cdot (g(|\nabla G_\sigma * I|)\nabla I). \tag{3}$$

We will refer to (3) as *modified Perona Malik* model in the course of this paper.

Another, geometrical generalization of (1) was suggested by Alvarez, Lions and Morel [9]

$$I_t = g(|\nabla G_\sigma * I|)|\nabla I|\nabla \cdot \left(\frac{\nabla I}{|\nabla I|}\right). \tag{4}$$

Since the right hand side can be rewritten as $g(|\nabla G_\sigma * I|)I_{\eta\eta}$, where $I_{\eta\eta}$ represents the tangential component of ΔI, it provides a smoothing only in the direction orthogonal to the

image gradient and uses g as a wheighting term to slow down the diffusion on high image gradients. Since $K = \nabla \cdot \left(\frac{\nabla I}{|\nabla I|} \right)$ is the mean curvature of level sets of I, (4) represents a geometrical diffusion of the image isosurfaces driven by their mean curvature, with an image dependent stopping function g. We call this model *slowed mean curvature flow*.

The last equation which we consider in this paper is so-called *geodesic mean curvature flow*

$$I_t = g(|\nabla G_\sigma * I|)|\nabla I|K + \nabla g(|\nabla G_\sigma * I|) \cdot \nabla I, \qquad (5)$$

which can be derived from (4) by adding the image dependent advective term. The equation was introduced simultaneously in [10], [11], [13] for image segmentation, for the filtering purposes (5) was suggested in [12], [17]. The image dependent velocity term drives the graylevel isosurfaces in the direction of $-\nabla g$, i.e. towards local edges. It can be written in divergence form

$$I_t = |\nabla I| \nabla \cdot \left(g(|\nabla G_\sigma * I|) \frac{\nabla I}{|\nabla I|} \right) \qquad (6)$$

to see (6) as a geometrical generalization of (2).

III. IMAGE DENOISING

We have applied the models introduced in the previous section to an in vivo zebrafish embryo nuclei and membranes 3-D images acquired with a confocal microscope Leica SP2 AOBS. Every volume has a size of 512x512x30 voxels, with a spacing of 0.58x0.58x1.04 μ^3. The data represent stages of development of zebrafish embryo nuclei and membranes that cover a period 4-6 hours, from the sphere to the shield stage. In the entire period of development, the whole embryo is similar to a sphere with a diameter of 700 μ. The data have a physical dimension of 300 x 300 x 30 μ^3 and cover only the top part of the embryo.

The nuclei data are composed of well contrasted objects, with an enough good signal to noise ratio and regions approximately uniform. The membranes images are more complex and difficult to handle. They are hollow and form an "interlacement" continuos in the whole volume. Very often the constrast is very low or the fluorescent signal is completely absent. The membranes thickness is very small, in the best case composed by no more than $3, 4$ voxels. Therefore, we adopted a different strategy, depending on the kind of data, to represent the image features.

As introduced in the previous section, in all the methods we use, the image features are given through the function g. In the case of nuclei we represent g as a standard edge indicator, i.e., as a smooth nonincreasing function of the original image gradient,

$$g(\mathbf{x}) = \frac{1}{1 + \frac{(G*\nabla I)^2}{\beta}} \, . \qquad (7)$$

However, for the membranes g, we found useful to express it as a smooth nonincreasing function of the image intensity, namely

$$g(\mathbf{x}) = \frac{1}{1 + \frac{(G*I)^2}{\beta}} \, . \qquad (8)$$

In both (7) and (8) the Gaussian variance acts like a scale parameter that determines the minimal size of details that can be preserved. The parameter β is instead related to the image contrast and it acts like a scale parameter by which the graylevels of the image features are mapped into the g function.

By using (8), we leave the useful signal of membranes unaltered as much as possible. Indeed, despite of the fact that (7) strongly reduces the noise, it smooths excessively the membranes. This behaviour is particularly evident where the signal is weak and the thickness of the membranes is thin. An example is shown in Fig. 1. Although (7) removes slightly better the noise, the membranes appear blurred and part of the information is lost. We verified in [14] that such information about boundaries is important to correctly segment the membranes. Mathematical reliability of such nonlinear models for image processing where the edge indicator may depend on image intensity is given in [16].

Numerical schemes for solving presented PDEs models can be based either on the explicit, see e.g. [17], or the semi-implicit [6], [7], [8], [18] time discretizations and on the finite difference, finite volume or finite element space discretizations. Since in case of explicit schemes one has to take care about the CFL stability condition, we use semi-implicit schemes, that are unconditionally stable. For the nuclei images, the implementation of such schemes is described in details in [18].

IV. FILTERING RESULTS

In this section we discuss visually and quantitatively the behaviour of the models on nuclei images, while for membranes we discuss the results by visual inspection. In the Fig. 2 we show a detail of an isosurface representation of nuclei, whereas such kind of visualization is not appropriate for membranes, where the isosurfaces are never closed. A detail of a slice selected in the xy plane is shown in Fig. 3.

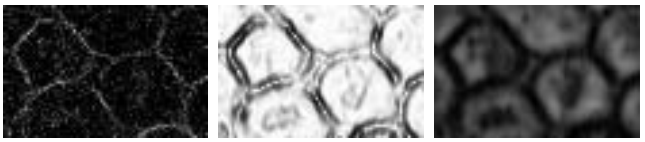

(a) Original data (b) Standard edge detector (c) New edge detector

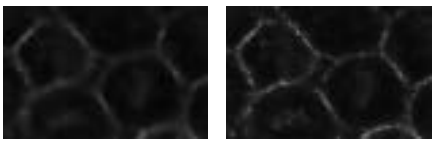

(d) Data filtered using eq.(7) (e) Data filtered using eq.(8)

Fig. 1. The original data and the edge indicators. On the bottom the data filtered using both functions.

Observing figures, we can see that all the methods reduce the noise superimposed to the image preserving at the same time its features. We used small values of variance σ in order to ehnance the contrast and preserve the small structures of membranes. The slowed mean curvature flow and the modified Perona-Malik models show good behaviour after 10 filtering steps, both for nuclei and membranes images, while the geodesic mean curvature flow requires 15 filtering steps. In all the computations our voxel size $h = 0.01$. Then the time step $\tau = 0.0001$ (to be close to relation $\tau \approx h^2$ which is standard for solving parabolic equations). In Fig. 2 we used further parameters as follows: $\beta = 2, \sigma = 5 \cdot 10^{-4}$ for the modified Perona-Malik and smcf models, $\beta = 1, \sigma = 10^{-3}$ for gmcf model. For filtering the membrane images presented in Fig. 3 we used $\beta = 10^{-3}, \sigma = 10^{-4}$ for the modified Perona-Malik and smcf models, while $\beta = 10^{-4}, \sigma = 5 \cdot 10^{-4}$ for gmcf model.

Concerning membrane images, it is worth to note that, although the noise intensity is often comparable with the intensity of membranes and the thickness of membranes is very small, the methods are able to distinguish between the noise inside membranes and the membranes itself. Visually the behaviour of all the methods is really satisfactory and comparable. To find a way how to evaluate quantitatively the filtering by different methods for this kind of data will be an objective of our further research.

Concerning nuclei images, by the visual inspection, cf. Fig. 2, we can conclude that the methods strongly reduce the noise and smooth small variations in image intensity without changing the shape of nuclei. However, we would like to compare the models also quantitatively. To that goal, we have selected a subvolume of the first unfiltered frame of the embryogenesis time sequence and constructed a gold standard by a manual segmentation. Then we calculated the mean Hausdorff distance[20] between the manually segmented surface of nuclei in the gold standard and isosurfaces of original and filtered data, respectively.

Given two finite point sets, $A = \{a_1, \ldots, a_p\}$ and $B = \{b_1, \ldots, b_q\}$ the *mean Hausdorff distance* is defined as

$$MHD(A, B) = \max\left(mhd(A, B), mhd(B, A)\right),$$

where

$$mhd(A, B) = \frac{1}{p} \sum_{i=1}^{p} \min_{b \in B} \|a_i - b\|$$

is called *mean directed Hausdorff distance* and $\|\cdot\|$ is some underlying norm (usually Euclidean) on the points of sets A, B. The $mhd(B, A)$ is defined similarly. The mean Hausdorff distance is widely used to measure the mismatch between two point sets usually to perform an image matching. In our case the sets A and B are given by discrete points that forms the nuclei surface in the gold standard and the image intensity isosurfaces either in original or in filtered volumes, respectively.

An appropriate image filtering should produce not only image smoothing and noise removal but also image enhancement. Then the level sets of the image intesity should

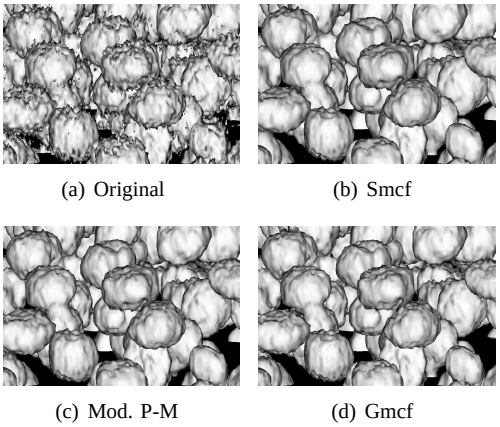

(a) Original (b) Smcf

(c) Mod. P-M (d) Gmcf

Fig. 2. Isosurface representation of original and filtered nuclei (by isosurface value 28).

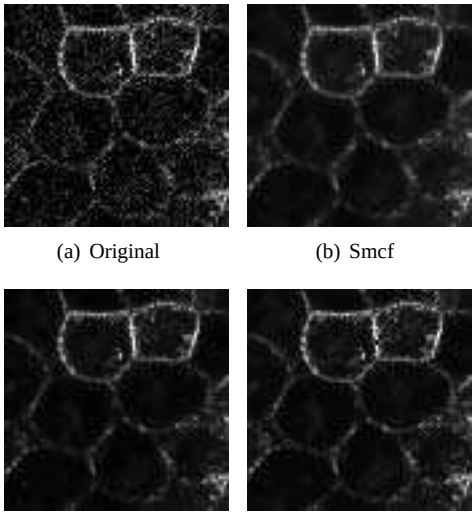

(a) Original (b) Smcf

(c) Mod. P-M (d) Gmcf

Fig. 3. A slice in the xy plane of original and filtered membranes. The slice has been selected in the middle of volumes.

accumulate around the boundaries of nuclei. The ideal image smoothing and enhancement would give a profile of image intensity perfectly steep on the nuclei boundaries.

Such profile would correspond to a totally flat graph of the mean Hausdorff distance. Therefore, by means of the mean Hausdorff distance to gold standard computed for the original and filtered data, it is possible to quantitavely evaluate the capability of smoothing and enhancement of the methods. Particularly, a reduction of the MHD by filtering shows the capability of smoothing, while the flatness of the MHD graph is related to enhancement.

Observing the image histogram and by the visual inspection we estimated the level of intensity 28 as the closest to the real boudaries of nuclei. We selected isosurface levels around this value, from 15 to 45, with step 5, in order to evaluate the mean Hausdorff distances. For every such isosurface either in original or filtered data, we found a nucleus surface in the gold standard and we calculated their mean Hausdorff distance. At the end we averaged the mean

Hausdorff distances over all nuclei in the subvolume. To check correct selection of the pairs of nuclei in the gold standard and other data we visualize them overlapped within their bounding boxes, see Fig. 4 in case of original data. The values of the mean Hausdorff distances are reported in Table I, and Fig. 4 shows the related graphs. We can easily observe that our choice of isosurface value 28 as the closest to the real boundaries of nuclei has been correct. In the original data, the isosurfaces with values between 25 and 30 give the smallest (and approximately the same) mean Hausdorff distance to the gold standard. This fact is expressed in almost flat graph of the mean Hausdorff distance in this interval. It is worth to note that the interval of the flatness for original data is very narrow (in spite of the graphs for modified Perona-Malik, smcf and gmcf filtering results), which means that correct representation of nuclei in the noisy data is very sensitive to the choice of correct isosurface level. Let us note that all the methods show good capability of smoothing, the mean Hausdorff distance with respect to the gold standard is reduced in the whole range of chosen isosurfaces. The graph of the slowed mean curvature flow is almost parallel to that of original data, meaning that it performs a pure edge preserving smoothing. The graph of modified Perona-Malik method is similar, but less convex and slightly more flat for lower isourfaces. Therefore, this method tends to more accumulate the image graylevels in that range of image intensity. The regions closely outside the nuclei contour moves towards the nuclei boundaries. This kind of behaviour is very strong in the geodesic mean curvature flow, that completely flatten the regions of a low intensity, enhancing thus edge position around nuclei. Further details and deep discussion about the evaluation of such methods using the mean Hausdorff distance can be found in [18].

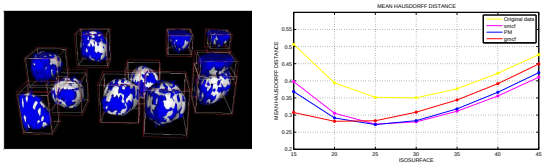

Fig. 4. Left: the plot of 11 nuclei of the gold standard (white) overlapped with the corresponding component of isosurface 25 in the original data set (blue). Right: the graph of the mean Hausdorff distance for the original and filtered data.

TABLE I

Mean Hausdorff Distance

Isosurface	Original	SMCF	PM	GMCF
15	0.506	0.411	0.369	0.308
20	0.394	0.302	0.292	0.282
25	0.352	0.265	0.272	0.283
30	0.350	0.274	0.284	0.308
35	0.377	0.313	0.318	0.344
40	0.422	0.364	0.367	0.392
45	0.476	0.429	0.424	0.449

V. CONCLUSIONS

In this paper we have presented PDEs edge preserving denoising methods and we applied them to 3-D confocal images of zebrafish embryo. We have introduced a modified version of classical edge detector to filter membranes data. Our study shows that nonlinear diffusion methods are well suited for processing such type of data. Using the mean Hausdorff distance measurement we show their good capabilities for smoothing and enhancement as well.

VI. ACKNOWLEDGMENTS

We thank all the members of the Embryomics and BioEmergences projects for our very fruitful interdisciplinary interaction.

REFERENCES

[1] S.Megason and S.Fraser, "Digitizing life at the level of the cell: high-performance laser-scanning microscopy and image analysis for in toto imaging of development," *Mech. Dev.*, vol.120, pp.1407-1420, 2003.

[2] J.J.Koenderink, "The structure of images", *Biol. Cybern.*, vol. 50, 1984, pp. 363-370.

[3] A.P.Witkin, "Scale-space filtering", *Proc. Eight Internat. Conf. on Artificial Intelligence*, vol. 2, 1983, pp.1019-1022.

[4] P.Perona, J.Malik, "Scale space and edge detection using anisotropic diffusion", *Proc. IEEE Computer Society Workshop on Computer Vision*, 1990.

[5] V.Catté et al., "Image selective smoothing and edge detection by nonlinear diffusion", *SIAM J. Numer. Anal.*, vol.29, 1992, pp.182-193.

[6] J.Kačur, K.Mikula, "Solution of nonlinear diffusion appearing in image smoothing and edge detection", *Applied Numerical Mathematics*, vol.17, 199, pp.47-59.

[7] K.Mikula, N.Ramarosy, "Semi-implicit finite volume scheme for solving nonlinear diffusion equations in image processing", *Numerische Mathematik*, vol.89, No.3, 2001, pp.561-590

[8] Z.Kriva, K.Mikula, "An adaptive finite volume scheme for solving nonlinear diffusion equations in image processing", *Journal for Visual Communication and Image Representation*, vol.13, No.1/2, 2002, pp.22-35

[9] L.Alvarez et al., "Image selective smoothing and edge detection by nonlinear diffusion II", *SIAM J. Numer. Anal.*, vol.29, 1992, pp.845-866.

[10] V.Caselles, R.Kimmel, G.Sapiro, "Geodesic active contours", *International Journal of Computer Vision*, vol.22, 1997, pp.61-79.

[11] S.Kichenassamy, A.Kumar, P.Olver, A.Tannenbaum, A.Yezzi, "Conformal curvature flows: from phase transitions to active vision", *Arch. Rational Mech. Anal.*, vol.134, 1996, pp.275-301

[12] Y.Chen, B.C.Vemuri, L.Wang, "Image denoising and segmentation via nonlinear diffusion", *Computers and Mathematics with Applications*, vol.39, 2000, pp.131-149.

[13] R.Malladi, J.Sethian, "Level Set Methods for curvature flow, image enhancement and shape recovery in medical images" *Visualization and Mathematics: Experiments, Simulations and Environements*, Eds. H. C. Hege, K. Polthier, pp.329-345, Springer Verlag, Heildelberg, 1997.

[14] C.Zanella et al., "Segmentation of Cells from 3D Confocal Images of Live Zebrafish Embryo", *to appear in EMBS 2007 Proceedings.*

[15] C.Melani et al., "Cells Tracking in a Live Zebrafish Embryo", *to appear in EMBS 2007 Proceedings.*

[16] J.Kačur, K.Mikula, "Slow and fast diffusion effects in image processing", *Computing and Visualization in Science*, vol.3, no.4, 2001, pp.185-195.

[17] A.Sarti, C.Ortiz de Solorzano, S.Lockett and R.Malldi, "A unified geometric model for 3D confocal image analysis in cytology", *IEEE Trans.On Biomedical Engineering*, vol.47, 2000, pp.1600-1609.

[18] Z.Kriva, K.Mikula, N.Peyrieras, B.Rizzi, A.Sarti, "3D early embryogenesys image filtering by nonlinear partial differential equations", submitted

[19] L.Alvarez et al., "Axioms and Fundamental Equations of Image Processing", *Archive for Rat. Mech. Anal.*, vol.123, 1993, pp.200-257.

[20] J.W.Zhang, G.Q.Han and Y.Wo, "Image Registration based on Generalized and Mean Hausdorff Distances" *Proceedings of the Fourth International Conference on Machine Learning and Cybernetics*, Guangzhou, 18-21 August 2005.